


## RESEARCH ARTICLE

# Endoplasmic reticulum-stress and unfolded protein response-activation in immune-mediated necrotizing myopathy

Corinna Preusse<sup>1,2</sup> | Theodore Marteau<sup>3</sup> | Norina Fischer<sup>1</sup> | Andreas Hentschel<sup>4</sup> | Albert Sickmann<sup>4</sup> | Sven Lang<sup>5</sup> | Udo Schneider<sup>6</sup> | Ulrike Schara-Schmidt<sup>3</sup> | Nancy Meyer<sup>3</sup> | Tobias Ruck<sup>7</sup> | Nora F. Dengler<sup>8</sup> | Johannes Prudlo<sup>9,10,11</sup> | Ales Dudesek<sup>9</sup> | Norman Görl<sup>12</sup> | Yves Allenbach<sup>13</sup> | Olivier Benveniste<sup>13</sup> | Hans-Hilmar Goebel<sup>1,14</sup> | Carsten Dittmayer<sup>1</sup> | Werner Stenzel<sup>1</sup>  | Andreas Roos<sup>3,15</sup>

<sup>1</sup>Department of Neuropathology, Charité - Universitätsmedizin Berlin, Corporate Member of Freie Universität Berlin and Humboldt-Universität zu Berlin, Berlin, Germany

<sup>2</sup>Department of Neurology with Institute for Translational Neurology, University Hospital Münster, Münster, Germany

<sup>3</sup>Pediatric Neurology, University Children's Hospital, Faculty of Medicine, University of Duisburg-Essen, Essen, Germany

<sup>4</sup>Leibniz-Institut für Analytische Wissenschaften - ISAS - e.V, Dortmund, Germany

<sup>5</sup>Department of Medical Biochemistry and Molecular Biology, Saarland University, Homburg, Germany

<sup>6</sup>Department of Rheumatology, Charité - Universitätsmedizin Berlin, Corporate Member of Freie Universität Berlin and Humboldt-Universität zu Berlin, Berlin, Germany

<sup>7</sup>Department of Neurology, Medical Faculty, Heinrich-Heine-University, Düsseldorf, Germany

<sup>8</sup>Department of Neurosurgery, Charité - Universitätsmedizin Berlin, Corporate Member of Freie Universität Berlin and Humboldt-Universität zu Berlin, Berlin, Germany

<sup>9</sup>Department of Neurology, Rostock University Medical Center, Rostock, Germany

<sup>10</sup>German Center for Neurodegenerative Diseases (DZNE) Rostock/Greifswald, Rostock, Germany

<sup>11</sup>Department of Neurology, University of Rostock, Rostock, Germany

<sup>12</sup>Department of Internal Medicine, Klinikum Südstadt Rostock, Rostock, Germany

<sup>13</sup>Department of Internal Medicine and Clinical Immunology, Sorbonne Université, APHP, Pitié-Salpêtrière University Hospital, Paris, France

<sup>14</sup>Department of Neuropathology, University Hospital Mainz, Mainz, Germany

<sup>15</sup>Children's Hospital of Eastern Ontario Research Institute, Ottawa, Ontario, Canada

## Correspondence

Werner Stenzel, Department of Neuropathology, Charité - Universitätsmedizin Berlin, Charitéplatz 1, Berlin 10117, Germany.  
Email: [werner.stenzel@charite.de](mailto:werner.stenzel@charite.de)

## Funding information

AFM-Téléthon, Grant/Award Number: 23216; Bundesministerium für Bildung und Forschung; European Regional Development Fund, Grant/Award Number: NME-GPS; Ministerium für Innovation, Wissenschaft und Forschung des Landes Nordrhein-Westfalen

## Abstract

Patients suffering from immune-mediated necrotizing myopathies (IMNM) harbor, the pathognomonic myositis-specific auto-antibodies anti-SRP54 or -HMGCR, while about one third of them do not. Activation of chaperone-assisted autophagy was described as being part of the molecular etiology of IMNM. Endoplasmic reticulum (ER)/sarcoplasmic reticulum (SR)-stress accompanied by activation of the unfolded protein response (UPR) often precedes activation of the protein clearance machinery and represents a cellular defense mechanism toward restoration of proteostasis. Here, we show that ER/SR-stress may be part of the molecular etiology of IMNM. To address this assumption, ER/SR-stress related key players covering the three known branches (PERK-mediated, IRE1-mediated, and ATF6-mediated) were investigated on both, the transcript and the protein levels utilizing 39 muscle biopsy

Corinna Preusse, Theodore Marteau, Norina Fischer, Werner Stenzel, and Andreas Roos contributed equally to the manuscript.

This is an open access article under the terms of the [Creative Commons Attribution-NonCommercial-NoDerivs](https://creativecommons.org/licenses/by-nc-nd/4.0/) License, which permits use and distribution in any medium, provided the original work is properly cited, the use is non-commercial and no modifications or adaptations are made.

© 2022 The Authors. *Brain Pathology* published by John Wiley & Sons Ltd on behalf of International Society of Neuropathology.

specimens derived from IMNM-patients. Our results demonstrate an activation of all three UPR-branches in IMNM, which most likely precedes the activation of the protein clearance machinery. In detail, we identified increased phosphorylation of PERK and eIF2 $\alpha$  along with increased expression and protein abundance of ATF4, all well-documented characteristics for the activation of the UPR. Further, we identified increased general *XBP1*-level, and elevated XBP1 protein levels. Additionally, our transcript studies revealed an increased *ATF6*-expression, which was confirmed by immunostaining studies indicating a myonuclear translocation of the cleaved ATF6-form toward the forced transcription of UPR-related chaperones. In accordance with that, our data demonstrate an increase of downstream factors including ER/SR co-chaperones and chaperones (e.g., SIL1) indicating an UPR-activation on a broader level with no significant differences between seropositive and seronegative patients. Taken together, one might assume that UPR-activation within muscle fibers might not only serve to restore protein homeostasis, but also enhance sarcolemmal presentation of proteins crucial for attracting immune cells. Since modulation of ER-stress and UPR via application of chemical chaperones became a promising therapeutic treatment approach, our findings might represent the starting point for new interventional concepts.

#### KEYWORDS

auto-antibodies, ER-stress, HMGCR, IMNM, SRP, UPR

## 1 | INTRODUCTION

Immune-mediated necrotizing myopathies (IMNM) are part of the idiopathic inflammatory myopathies, which were defined precisely by international consensus recently [1, 2]. Diagnostic criteria of IMNM were based on clinical, morphological as well as serological features [1]. The main characteristics include proximal lower limb-predominant muscle weakness, substantially increased serum CK levels, and detection of the pathognomonic myositis-specific auto-antibodies anti-SRP54 or -HMGCR in most patients, while 1/3 of IMNM patients do not harbor them. Both auto-antibodies target proteins of the endoplasmic reticulum (ER)/sarcoplasmic reticulum (SR) and are detectable in sera of myositis patients [3]. Morphologically, IMNM patient's affected skeletal muscles show diffusely distributed myofiber necrosis, regenerating muscle fibers and sarcolemmal expression of MHC class I. Furthermore, a sarcolemmal complement deposition (C5b-9) is found on a variable proportion of myofibers, supporting the pathogenicity of the autoantibodies, as well as relatively few endomysial T cells showing signs of exhaustion, but not of terminal differentiation [4]. Additionally, small, non-rimmed vacuoles may be detected. Such vacuoles were recently characterized in more detail, and inflammation-driven activation of the chaperone-assisted autophagy appears to be involved in IMNM-pathogenesis [5]. Notably, ER-stress and UPR-activation often precedes activation of the cellular protein clearance machinery including autophagy [6]. ER/SR-stress accompanied by the activation of the unfolded protein response (UPR) represents a cellular defense mechanism toward restoration of

proteostasis and has been linked to the pathophysiology of a variety of (inherited) neurological diseases including those affecting skeletal musculature such as Marinesco-Sjögren syndrome, *SEPN1*-related myopathy and *RYR1*-mediated core myopathy [7, 8]. In general, the UPR has three aims: (i) restoration of cellular homeostasis by pausing and adjusting protein translation, (ii) enhancing degradation of misfolded proteins from the ER/SR, and (iii) activation of signaling pathways leading to increased production of molecular chaperones facilitating protein folding [9]. The UPR is orchestrated by three different so-called UPR-branches: PERK-mediated, IRE1-mediated, and ATF6-mediated. It is important to note that these branches are controlled by BiP (GRP78), which dissociates from these proteins toward their activation and serving as a major chaperone itself [10]. Perturbed ER-function and UPR-activation are often associated with a transportation of misfolded proteins across the ER/SR membrane into the cytoplasm/sarcoplasm targeted for proteolysis by the proteasome and / or the autophagic flux [11].

Given that altered protein clearance capacity is often accompanied by perturbed ER/SR-homeostasis, we hypothesize that ER/SR-stress may be part of the molecular pathomechanism of IMNM. To systematically address this assumption, proteomic signature of quadriiceps muscle derived from IMNM-patients was filtered for proteins involved in protein processing, modulation of ER/SR-stress and protein (re-)folding, as well as protein clearance. This approach confirmed the previously published presence of an activated protein clearance machinery in IMNM-patient derived muscle [5], and,

moreover, suggested the presence of ER/SR-stress and UPR-activation. To further investigate this in the pathobiochemistry of IMNM, ultrastructural studies were carried out and ER/SR-stress related key players covering the three known branches modulating the cellular stress response were investigated on both, the gene transcript and the protein levels utilizing muscle biopsy specimens derived from IMNM-patients presenting with auto-antibodies against SRP54 or HMGCR or autoantibody-negative, respectively. Given that (i) the presence of vacuoles (as verified by electron microscopy) might suggest the presence of degenerative mechanisms or pathomechanisms not directly related to immunology and that (ii) IMNM-patients (in contrast to patients suffering from dermatomyositis and anti-synthetase syndrome) for unknown reasons often present with poor muscle strength recovery, one might assume that these patients benefit from drugs targeting the protein processing and clearance machinery such as chemical chaperones.

## 2 | MATERIAL AND METHODS

### 2.1 | Patients

Clinical data of all patients enrolled in this study are listed in Table 1. We included patients with typical clinical, serological, and morphological signs and symptoms of immune-mediated necrotizing myopathy diagnosed according to the clinico-sero-morphological European Neuromuscular Centre (ENMC) criteria [3], either with SRP54 or HMGCR autoantibodies or without detectable antibodies. Additionally, we included sex- and age-matched individuals defined as non-diseased controls (NDCs) in the analyses. The latter ones had undergone a muscle biopsy because of nonspecific complaints, but were found not to have any inflammatory muscle disease. Their CK levels were normal and no signs of systemic inflammation and no myositis-specific antibodies or myositis-associated antibodies were detectable. Informed consent was obtained from all patients and the Charité

TABLE 1 Clinical information

	IMNM			IBM	NDC
	SRP	HMGCR	AB negative or unknown <sup>a</sup>	MUP44±	MSA/MAA negative
<i>n</i>	14	19	6	8	9
Age (years)	45.3 ± 15.1	60.9 ± 23	69.6 ± 10	79.0 ± 6.3	49.5 ± 10
Gender					
Female	86% (12)	68% (13)	33% (2)	50% (4)	56% (5)
Male	7% (1)	26% (5)	50% (3)	50% (4)	22% (2)
Unknown	7% (1)	5% (1)	17% (1)		22% (2)
CK level					
Normal	7% (1)				100% (9)
2-10-fold	7% (1)	26% (5)	33% (2)	75% (6)	
>10-fold	71% (10)	63% (12)	33% (2)	13% (1)	
Unknown	14% (2)	11% (2)	33% (2)	13% (1)	
Time since onset					
<1 year	64% (9)	53% (10)	33% (2)		66% (6)
1-5 years	29% (4)	26% (5)	17% (1)	25% (2)	33% (3)
>5 years		11% (2)		75% (6)	
Unknown	7% (1)	11% (2)	17% (1)		
Symptoms					
Proximal weakness	87% (13)	95% (18)	83% (5)		
+ Tetraparesis		21% (4)	17% (1)		
Dysphagia	7% (1)			25% (2)	
IBM pattern				100% (8)	
Other or additional organs involved	36% (5)	16% (3)			
Subjective weakness/fatigability					100% (9) <sup>b</sup>
Unknown	7% (1)	5% (1)	17% (1)		

Note: Clinical information of IMNM patients split according to antibody subgroups.

Abbreviations: IMNM, immune-mediated necrotizing myopathies; MAA, myositis-associated antibodies; MSA, myositis-specific antibodies; NDC, non-diseased control.

<sup>a</sup>From these six patients: one is negative for SRP and HMGCR, two are negative for SRP, while HMGCR was not tested (since the antibody was not available at time of diagnosis), and from three patients no information about the test status could be obtained.

<sup>b</sup>Weakness and fatigability were described by patients; however, no objective weakness was measurable by clinical examination.

(EA2/163/17) and Essen (10-9011-BO) ethics committee had granted ethical approval.

## 2.2 | Skeletal muscle specimens

In this study, we analyzed biopsied skeletal muscles derived from 39 IMNM patients, IBM patients ( $n = 8$ ) as disease-control group and ( $n = 10$ ) NDCs. Because of numeric variation of availability of patient tissues for certain methods and subgroups, numbers of patients per subgroup are as follows: histology,  $n = 3-5$ , qPCR transcript analyses,  $n = 9-15$ , proteomic analysis,  $n = 6$ . All skeletal muscle specimens were cryopreserved at  $-80^{\circ}\text{C}$  prior to analyses.

## 2.3 | Morphological analysis

All stains were performed on  $8\ \mu\text{m}$  cryo-microtome sections, according to standard procedures. Immunohistochemical and immunofluorescence staining procedures were carried out as described previously [12, 13]. The following antibodies were used: ATF4, ATF6, BiP, CALR, GRP94, GRP170, PDIA2, PDIA3, pEIF2a, pIRE1, pPERK, XBP1, for details see Table S1.

## 2.4 | Large-scale electron microscopy

Four muscle biopsies (two biopsies from patients with SRP54 and two with HMGCR auto-antibodies) were embedded for transmission electron microscopy according to a standard protocol and used to perform large-scale electron microscopy as recently described [14]. Briefly, ultrathin sections with virtual absence of limiting artifacts (large-scale digitization samples) were prepared and entirely digitized with a Zeiss Gemini 300 scanning electron microscopy in transmission mode at  $5\ \text{nm}$  pixel size. Bigtif files were generated with Fiji/TrakEM2 [15] and nip2 and analyzed in QuPath [16].

## 2.5 | Quantitative reverse transcription PCR (qRT-PCR)

Total RNA was extracted from muscle specimens using the technique described previously [12]. Briefly, cDNA was synthesized using the High-Capacity cDNA Archive Kit (Applied Biosystems). For qPCR reactions,  $10-20\ \text{ng}$  of cDNA were used, and for subsequent analysis, the QuantStudio 6 Flex System (Applied Biosystems) was utilized with the following, running conditions:  $95^{\circ}\text{C}$  0:20,  $95^{\circ}\text{C}$  0:01,  $60^{\circ}\text{C}$  0:20, 45 cycles (values above 40 cycles were defined as not expressed). All targeted transcripts were run as triplicates. For each of these runs, the reference gene *PGKI* has been included as internal

control to normalize the relative expression of the targeted transcripts. The TaqMan<sup>®</sup> Gene Exp Assay from Life Technologies/ThermoFisher are listed as follows: *ATF4* Hs00909569\_g1, *ATF6* Hs00232586\_m1, *HSPA5* (BiP) Hs00607129\_gH, *CALR* Hs00376764\_m1, *CANX* Hs01558409\_m1, *EDEMI* Hs00976004\_m1, *ERN2* (EIF2) Hs01086607\_m1, *HSP90B1* (GRP94) Hs00427665\_g1, *HYOU1* (GRP170) Hs00197328\_m1, *ERN2/IRE1* Hs01086607\_m1, *PDIA2* Hs00429010\_m1, *PDIA3* Hs00607126\_m1, *EIF2AK3* (PERK) Hs00984003\_m1, *PGKI* Hs99999906\_m1, *SIL1* Hs00223835\_m1, *XBP1* Hs00231936\_m1. Displayed are fold change ( $2^{\Delta\Delta\text{CT}}$ ) of gene expression versus NDC values.

## 2.6 | Sample preparation for proteomics analysis

Muscle tissue was snap-frozen in liquid nitrogen and stored at  $-80^{\circ}\text{C}$  until usage. The total muscle was lysed with  $200\ \mu\text{l}$  of  $50\ \text{mM}$  Tris-HCl (pH 7.8) buffer, containing 5% SDS, and complete ULTRA protease inhibitor (Roche) using the Bioruptor<sup>®</sup> (Diagenode) for 10 min (30 s on, 30 s off, 10 cycles) at  $4^{\circ}\text{C}$ . To ensure complete lysis, an additional sonication step using an ultra-sonic probe (30 s, 1 s/1 s, amplitude 40%) followed by centrifugation at  $4^{\circ}\text{C}$  and  $20,000\ \text{g}$  for 15 min was conducted. Protein concentration of the supernatant was determined by BCA assay according to the manufacturer's protocol. Disulfide bonds were reduced by the addition of  $10\ \text{mM}$  TCEP at  $37^{\circ}\text{C}$  for 30 min. Free sulfhydryl bonds were alkylated with  $15\ \text{mM}$  IAA at room temperature in the dark for 30 min.  $100\ \mu\text{g}$  protein of each sample was used for proteolysis using the S-Trap protocol (Protifi) and using a protein to trypsin ratio of 20:1. The incubation time for trypsin was changed to 2 h at  $37^{\circ}\text{C}$ . Proteolysis was stopped using FA to acidify the sample (pH  $< 3.0$ ).

Proteolytic digests were checked for complete digestion after desalting by using monolithic column separation (PepSwift monolithic PS-DVB PL-CAP200-PM, Dionex) on an inert Ultimate 3000 HPLC (Dionex) by direct injection of  $1\ \mu\text{g}$  sample. A binary gradient (solvent A: 0.1% TFA, solvent B: 0.08% TFA, 84% ACN) ranging from 5% to 12% B in 5 min and then from 12% to 50% B in 15 min at a flow rate of  $2.2\ \mu\text{l}/\text{min}$  and at  $60^{\circ}\text{C}$ , was applied. UV traces were acquired at  $214\ \text{nm}$  [17].

## 2.7 | LC-MS/MS analysis

All samples were analyzed by nano LC-MS/MS using  $1\ \mu\text{g}$  of sample material. Samples were loaded on an Ultimate 3000 Rapid Separation Liquid chromatography nano system with a ProFlow flow control device coupled to a Fusion Lumos Tribrid mass spectrometer (both from Thermo Scientific). After initial loading, peptides were concentrated on a trapping column (Acclaim C18

PepMap100, 100  $\mu\text{m}$ , 2 cm) using 0.1% TFA at a flowrate of 10  $\mu\text{l}/\text{min}$ . Following sample separation was accomplished on a reversed phase column (Acclaim C18 PepMap100, 75  $\mu\text{m}$ , 50 cm) using a binary gradient: 3% solvent B (84% ACN with 0.1% TFA) for 10 min, a linear increase of solvent B to 35% for 120 min, a linear increase of solvent B to 95% for 10 min followed by a linear decrease of solvent B to 3% for 5 min. MS survey scans were acquired on the Fusion Lumos using settings as follows: mass spectrometer was operated in data dependent acquisition mode (DDA) with full MS scans from 300 to 1500  $m/z$  at a resolution of 120,000 (Orbitrap) using the polysiloxane ion at 445.12002  $m/z$  as lock mass. The automatic gain control (AGC) was set to 2E5 and the maximum injection time to 50 ms. The most intense ions above a threshold ion count of 5E3 were selected for fragmentation at a normalized collision energy of 30% (HCD) in each cycle of the acquisition analysis, following each survey scan. The dynamic exclusion time was set to 15 s. The number of selected precursor ions for fragmentation was determined by the “rapid” acquisition algorithm. Fragment ions were acquired in the linear ion trap with an AGC of 2E3 and a maximum injection time of 300 ms.

## 2.8 | Analysis of DDA data

Progenesis LC-MS software from Nonlinear Dynamics was used to analyze the label-free proteomic data. Only features which had a charge of +2, +3, and/or +4 were allowed for analysis. After this preliminary step, the MS/MS data were exported for protein identification. To minimize redundant MS/MS spectra, only features with  $\leq 10$  rank were exported as peak lists, which were searched against a concatenated target/decoy version of the human Uniprot database (downloaded on October 26, 2017 containing 20,226 target entries).

To increase the number of peptide spectrum matches (PSMs), that is, the number of detected peptide spectra matching a protein, a multiple search algorithm strategy was followed by using SearchGui [18], a software combining different protein identification algorithms. Thus, a total of three different search algorithms (Mascot, X!Tandem and Comet) were used in this work. The following basic parameters were applied equally to each database search: Trypsin was selected as the protease with a maximum of two missed cleavages allowed. The tolerance for precursor ion  $m/z$  values was set to 10 ppm, with a tolerance for fragment ions of 0.5 Da. In each case, searches were performed against the target/decoy version of the UniProt human database. Peptide modifications were set as carbamidomethylation of cysteine as fixed and oxidation of methionine as variable.

To combine the results of the different search algorithms, the PeptideShaker [19] software was used. In addition, it was used to filter and validate the data with 1% FDR at the level of PSMs, proteins, and peptides. The results processed in this way were then reimported

back into the Progenesis software to match the identified proteins and peptides to the appropriate spectra. Finally, a protein list was exported from Progenesis containing all proteins identified in the corresponding experiment with the number of specific peptides found.

For relative quantification, only proteins identified with two or more unique peptides were considered for further analysis. After this initial filtering, the average of the normalized abundances was calculated and used to determine the ratios between the overexpression model or patient samples with their respective controls including log<sub>2</sub> transformation and  $p$ -value generation by performing a Student's  $t$ -test.

## 2.9 | Statistical analysis

Since this is an exploratory and descriptive study, sample sizes are not based on a priori power calculation, but based on previous studies.

Data are presented as the mean  $\pm$  SEM in either dot blots or overlay of dot blots and Box-Whiskers blots. Differences between two means were examined by the Mann-Whitney  $U$  test in transcript levels. The level of significance was set at  $p < 0.05$ . GraphPad Prism 9.0.1 software (GraphPad Software, Inc.) was used for statistical analysis.

## 3 | RESULTS

### 3.1 | Clinical information of the patients' cohort

In this study, 39 adult patients with IMNM either SRP54 auto-antibody-positive ( $n = 14$ ), HMGCR auto-antibody-positive ( $n = 18$ ) or without known antibody status ( $n = 7$ ) were enrolled. SRP54<sup>+</sup> patients were 45.3 years old and 86% females, while HMGCR<sup>+</sup> patients had a mean age of 63.2 years and 72% were female. CK was very high in most patients ( $>10$ -fold in SRP54<sup>+</sup> and HMGCR<sup>+</sup> patients), although time of onset was mostly less than 1 year. The main symptom in IMNM patients was proximal weakness (87% in SRP54<sup>+</sup> and 94% in HMGCR<sup>+</sup> patients). CK-levels did not correlate with any gene expression data (data not shown). IMNM patients were compared to a disease-control group of typical IBM patients ( $n = 8$ , mean age 79.0 years, CK levels moderate, time since onset  $>5$  years) and a non-disease controls ( $n = 9$ , mean age 49.5 years, normal CK level and subjective weakness less than 1 year). All clinical data are displayed in Table 1.

### 3.2 | Proteomic profiling revealed dysregulation of ER/SR, proteasomal and chaperone-mediated autophagy proteins

Unbiased proteomic profiling of IMNM patient-derived muscle biopsies allowed for quantification of 1129

TABLE 2 Proteins found by unbiased proteomic profiling of IMNM patient-derived muscle biopsies.

Accession #	Unique peptides	Description	Ratio	p-value
<b>ER-stress</b>				
P27824	7	Calnexin (CALX_HUMAN)	3.89	0.00
P11021	14	78 kDa glucose-regulated protein (GRP78_HUMAN)	3.80	0.00
P27797	8	Calreticulin (CALR_HUMAN)	3.62	0.02
P16615	36	Sarcoplasmic/endoplasmic reticulum calcium ATPase 2 (AT2A2_HUMAN)	3.47	0.00
O14958	11	Calsequestrin-2 (CASQ2_HUMAN)	3.39	0.02
P30101	11	Protein disulfide-isomerase A3 (PDIA3_HUMAN)	3.16	0.02
Q86TD4	24	Sarcalumenin (SRCA_HUMAN)	2.94	0.00
P55072	27	Transitional endoplasmic reticulum ATPase (TERA_HUMAN)	2.86	0.00
O75298	8	Reticulon-2 (RTN2_HUMAN)	2.24	0.00
O14983	39	Sarcoplasmic/endoplasmic reticulum calcium ATPase 1 (AT2A1_HUMAN)	2.16	0.01
Q9HCP6	8	Protein-cysteine N-palmitoyltransferase HHAT-like protein (HHATL_HUMAN)	2.11	0.00
P31415	24	Calsequestrin-1 (CASQ1_HUMAN)	2.03	0.01
<b>Nuclear chaperones</b>				
O14558	8	Heat shock protein beta-6 (HSPB6_HUMAN)	11.11	0.02
Q9UBY9	8	Heat shock protein beta-7 (HSPB7_HUMAN)	4.55	0.00
Q16082	5	Heat shock protein beta-2 (HSPB2_HUMAN)	3.49	0.01
<b>Cytosolic chaperones</b>				
P08238	11	Heat shock protein HSP 90-beta (HS90B_HUMAN)	5.95	0.00
P31948	11	Stress-induced-phosphoprotein 1 (STIP1_HUMAN)	5.51	0.00
Q81WX7	14	Protein unc-45 homolog B (UN45B_HUMAN)	4.12	0.00
P04792	20	Heat shock protein beta-1 (HSPB1_HUMAN)	3.92	0.00
P0DMV8	22	Heat shock 70 kDa protein 1A (HS71A_HUMAN)	3.75	0.00
P07900	11	Heat shock protein HSP 90-alpha (HS90A_HUMAN)	3.40	0.00
P54652	9	Heat shock-related 70 kDa protein 2 (HSP72_HUMAN)	2.77	0.00
P11142	22	Heat shock cognate 71 kDa protein (HSP7C_HUMAN)	2.61	0.00
P02511	25	Alpha-crystallin B chain (CRYAB_HUMAN)	2.39	0.01
<b>Mitochondrial chaperones</b>				
P10809	19	60 kDa heat shock protein, mitochondrial (CH60_HUMAN)	2.57	0.00
P61604	6	10 kDa heat shock protein, mitochondrial (CH10_HUMAN)	2.27	0.00
<b>Proteolysis</b>				
P28070	5	Proteasome subunit beta type-4 (PSB4_HUMAN)	28.01	0.00
P22061	8	Protein-L-isoaspartate(D-aspartate) O-methyltransferase (PIMT_HUMAN)	4.86	0.00
P28074	6	Proteasome subunit beta type-5 (PSB5_HUMAN)	4.83	0.00
O95817	10	BAG family molecular chaperone regulator 3 (BAG3_HUMAN)	4.41	0.03
P22314	21	Ubiquitin-like modifier-activating enzyme 1 (UBA1_HUMAN)	4.11	0.00
O14818	5	Proteasome subunit alpha type-7 (PSA7_HUMAN)	3.60	0.00
P0CG47	5	Polyubiquitin-B (UBB_HUMAN)	3.41	0.00
P28066	2	Proteasome subunit alpha type-5 (PSA5_HUMAN)	3.27	0.00
P61088	7	Ubiquitin-conjugating enzyme E2 N (UBE2N_HUMAN)	2.86	0.00

(Continues)

TABLE 2 (Continued)

Accession #	Unique peptides	Description	Ratio	p-value
P60900	4	Proteasome subunit alpha type-6 (PSA6_HUMAN)	2.76	0.00
Q9UNZ2	4	NSFL1 cofactor p47 (NSF1C_HUMAN)	2.16	0.00

Note: We quantified 1129 proteins with 283 (25%) of them being statistically significantly regulated. Whereby 37 (13% of significantly regulated proteins; 3.3% of all abundant proteins) were directly involved in the modulation of ER/SR-stress, proteolysis or present with functions as nuclear, cytosolic or mitochondrial chaperones.

proteins with 283 (25%) of them being statistically significantly regulated. Interestingly, 37 of these (13% of significantly regulated proteins; 3.3% of all abundant proteins) were directly involved in the modulation of ER/SR-stress, proteolysis or present with functions as nuclear, cytosolic or mitochondrial chaperones (Table 2), thus indicating the presence of perturbed ER/SR-homeostasis in muscle cells of IMNM-patients.

### 3.3 | Ultrastructural findings analyzed by large-scale electron microscopy and TEM show autophagy and ER activation

In line with this assumption, we observed ultrastructural features of autophagy, with numerous muscle fibers showing both finely dispersed as well as larger groups of prominent autophagic compartments (Figure 1A,B). These compartments were consistent with autophagosomes showing granular material and mitochondria as well as autolysosomes with partially degraded material (Figure 1C–H) [20, 21]. Also, several fibroblasts and endothelial cells showed signs of activation with relatively large cell bodies and prominent ER and Golgi apparatus profiles (Figure 1I–K). Those alterations were studied also in a set of 11 specimens of anti-SRP<sup>+</sup> ( $n = 4$ ), anti-HMGCR<sup>+</sup> ( $n = 2$ ), and autoantibody-negative ( $n = 5$ ) IMNM by conventional TEM, and there were no quantitative differences discernible between these subgroups (data not shown). Ultrastructural abnormalities were unevenly and focally distributed within the specimens (exemplary visualization via double-immune-fluorescents see Figure S1).

### 3.4 | Broad activation of the UPR machinery in IMNM patients

Since it has been shown that in the pathobiochemistry of IMNM the chaperone-assisted selective autophagy (CASA) pathway is activated [5], and prompted by our proteomic findings mentioned above, we hypothesized that also ER/SR-stress is a major pathophysiological hallmark in these patients. As UPR-activation represents a cellular defense mechanism aiming at restoration of proteostasis after ER/SR-stress, we analyzed the three different UPR-branches in patient-derived muscle samples.

#### 3.4.1 | PERK-mediated UPR branch

Histological analyses demonstrated increased phosphorylation of PERK and eIF2 $\alpha$  in accumulated immune cells in both, anti-SRP54<sup>+</sup> and anti-HMGCR<sup>+</sup> IMNM patient's muscles (Figure 2A). In line with the known activation of PERK and eIF2 $\alpha$  via phosphorylation [22], levels of the corresponding transcripts are not elevated in IMNM-patient-derived muscles of all disease subgroups. However, *ATF4* transcript levels were slightly increased (2-fold) although not statistically significant (Figure 2B). In line with the increase of *ATF4* transcripts, also ATF4 protein levels were increased in immune cells of muscle from IMNM-patients compared to protein abundance in control muscles (Figure 2A).

#### 3.4.2 | IRE1-mediated UPR branch

Increased phosphorylation of IRE1, as well as increase of XBP1 protein was also identified by immunostaining and transcript studies, respectively. pIRE was found on myofibers and immune cells, while strong XBP1 staining was found in areas of intense immune cell infiltration (Figure 3A). In accordance, gene expression levels of *XBPI* were also increased more than 2-fold in about 40% of IMNM patient's muscles, independent from the underlying antibody subtype. However, overall mean expression was not significantly changed when compared to NDC, and expression level of *IRE1* (in line with the known activation via phosphorylation [22]) was not changed (Figure 3B).

#### 3.4.3 | ATF6-mediated UPR branch

ATF6 protein abundance is increased in the myonuclei of necrotic fibers, and (slightly) in immunologically active areas of the muscle, as well as intensely in immune cells (Figure 4A). Gene expression of this marker was significantly increased, again, without differences in the antibody subtypes (Figure 4B).

#### 3.4.4 | UPR-Chaperones

Important to note is that BiP (GRP78) acts either as chaperone or as primary sensor in the activation of the

UPR [23]. Direct interaction of BiP with IRE1 and PERK switches BiP from its chaperone cycle into an ER stress sensor cycle. Consequently, we analyzed BiP in our

cohort and identified a strong accumulation in immune cells (Figure 5A), while gene expression was additionally (only slightly) increased. BiP co-chaperones like SIL1

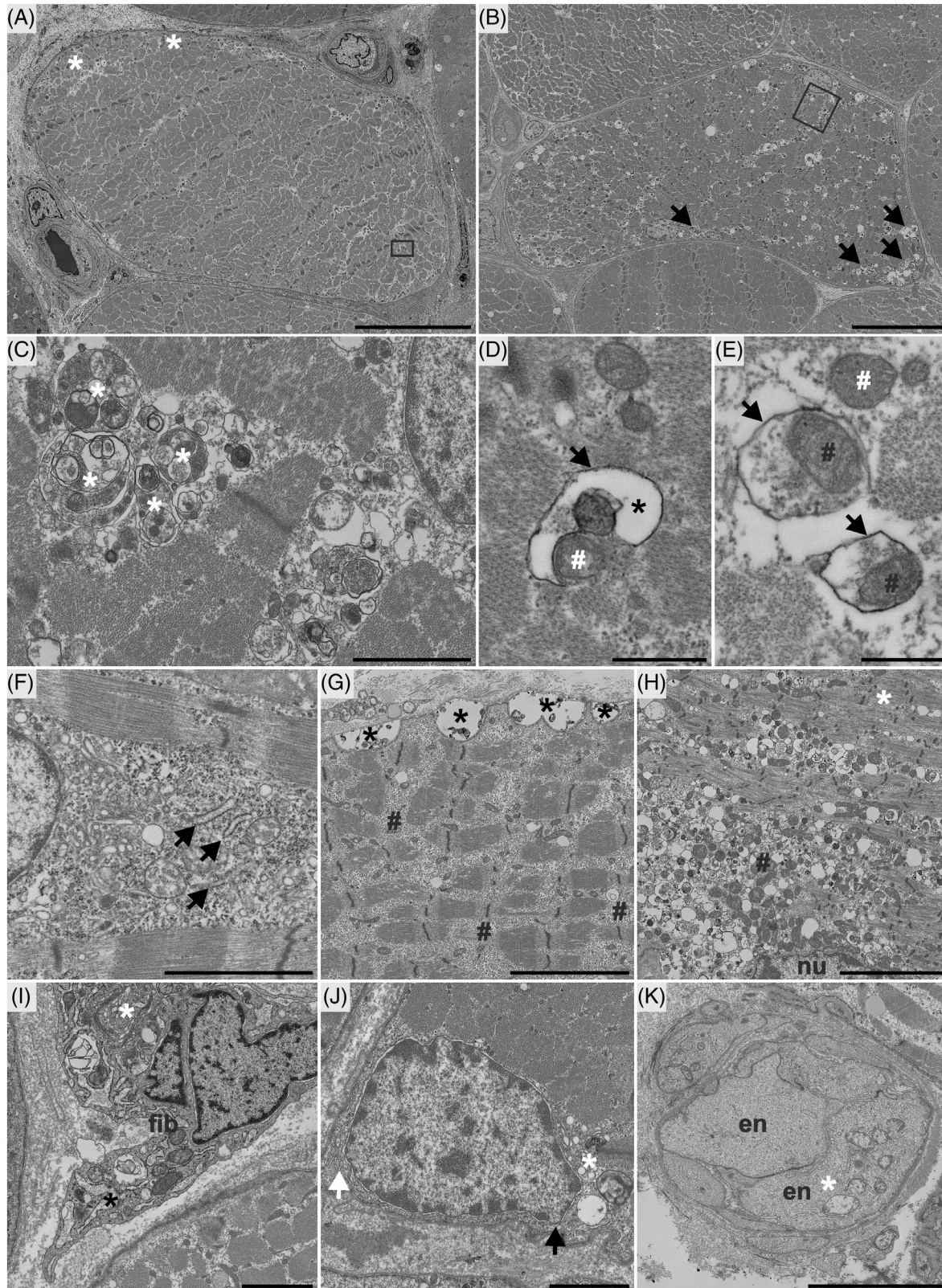
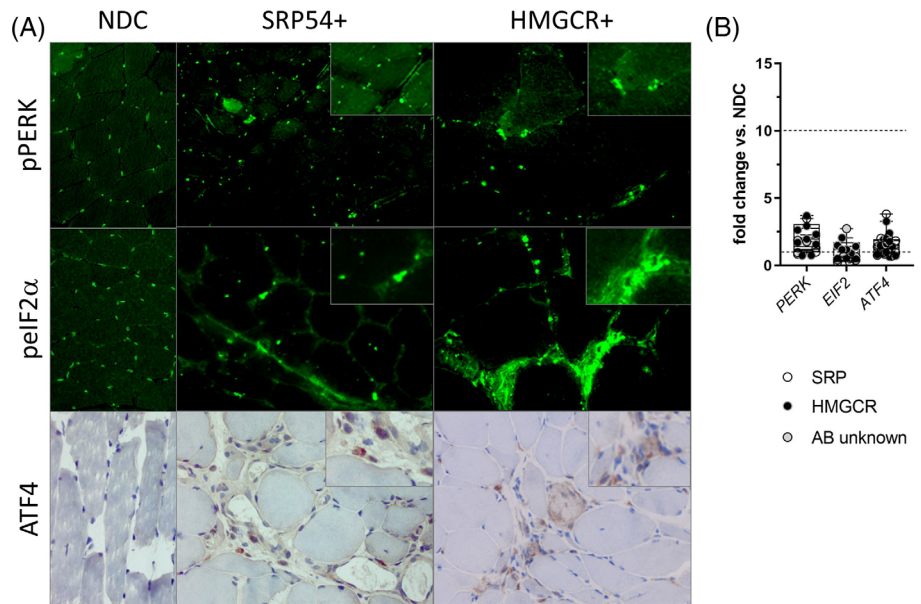


FIGURE 1 Legend on next page.



**FIGURE 2** PERK-mediated unfolded protein response branch is activated on protein, but not gene level. (A) Immunofluorescent and -histochemical staining revealing accumulation of pPERK, pEIF2 $\alpha$ , and ATF4 in immune-mediated necrotizing myopathies muscles predominantly on immune cells, independent of the underlying auto-antibody subtype. Original magnification 400 $\times$ . (B) Gene analysis of *PERK*, *EIF2*, *ATF4* shows no significant elevation compared to non-diseased control; however, gene expression of *ATF4* seems to be slightly elevated in some SRP<sup>+</sup> muscles. The level of significance was set to  $p < 0.05$ .



**FIGURE 3** XBP1 is highly activated on gene and protein level. (A) Immunofluorescent and -histochemical staining reveals mild accumulation of pIRE1 on myofibers and strongly on immune cells, while XBP1 is strongly on immune cells in immune-mediated necrotizing myopathies (IMNM) muscles as well, independent of the underlying auto-antibody subtype. Original magnification 400 $\times$ . (B) Gene analysis of *IRE1*, *XBP1* shows significant upregulation of *XBP1* gene expression in IMNM muscles when compared to non-diseased control. The level of significance was set to  $*p < 0.05$

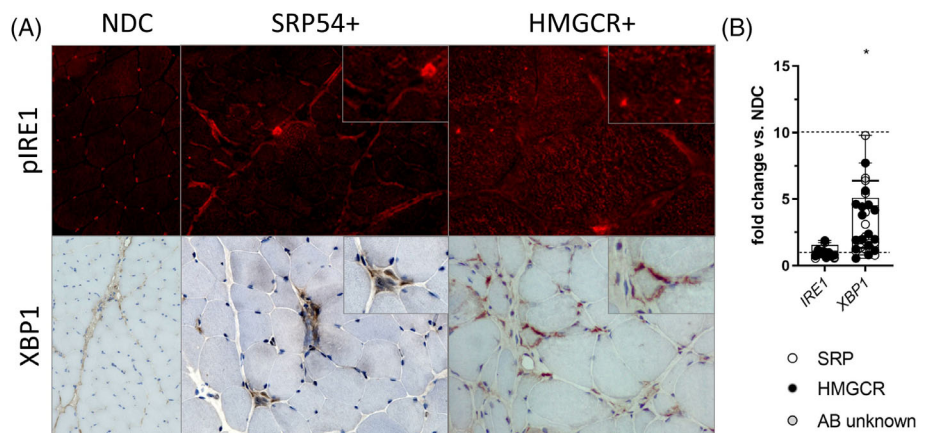


**FIGURE 1** Ultrastructural findings of biopsied skeletal muscle tissue with immune-mediated necrotizing myopathies, analyzed by large-scale electron microscopy. HMGCR<sup>+</sup> Pat 1 (A–E, I, J), SRP54<sup>+</sup> Pat (K), HMGCR<sup>+</sup> Pat 2 (F, G, H). Entire ultrathin sections were digitized at 5.0 nm pixel size; images show digitally magnified regions, except for D and E that were manually acquired at highest resolution. (A) Muscle fiber with very mild microanatomical alterations; focally, vacuolar structures can be discerned (asterisks). However, numerous autophagic compartments could be identified at high resolution (E; high-resolution image of the boxed area in A, showing two autophagosomes). (B) Muscle fiber with pronounced microanatomical alterations, showing numerous autophagic compartments. These are finely dispersed within the fiber and also show larger aggregates (arrows). The autophagic compartments consist of autophagosomes and autolysosomes, presenting with e.g. enclosed granular material and mitochondria (asterisks in C; digitally magnified region of the boxed area in B). (D) In another fiber, a membrane formation (the arrow points at the outer membrane) suggestive of a phagophore was identified, with a mitochondrion in direct proximity (#) and a prominent electron-lucent cisterna (asterisk). (E) Electron dense limiting membranes of the autophagosomes can be discerned (arrow), also mitochondria within the autophagosomes (black #) that, characteristically, demonstrate very similar electron density and structure as compared to a cytoplasmic mitochondrion (white #). However, in these two examples, no inner membrane can be discerned, maybe a preparation artifact or connected to autophagosome maturation. (F) Prominent membrane organelles such as the Golgi apparatus and rough endoplasmic reticulum (black arrows) are visible in the perinuclear region. (G) Several fibers showed a serrated surface because of numerous exocytosed cargo, which was especially prominent in longitudinal sections as shown here (multiple fibers also exhibited prominent granular material displacing the myofibrils, perhaps glycogen; #). (H) Several fibers exhibited a substantial amount of autophagic vacuoles; here, in this longitudinal section, myofibrils (asterisk) are displaced by the vacuoles (#) and show an altered and rarefied architecture (nu nucleus). (I) Some fibroblasts (fib) showed signs of activation with prominent rough endoplasmic reticulum (black asterisk) and Golgi apparatus (white asterisk). (J) Several myonuclei showed a prominent perinuclear cisterna (black arrow); note a transition toward multiple stacks of endoplasmic reticulum (white arrow) and the perinuclear Golgi apparatus (white asterisk). Some vessels demonstrated alterations; several appeared enlarged, while others (K) showed signs of activation with abundant granular material and large sized endothelial cells (en) as well as prominent organelles (asterisk). Scale bars: A, B: 15  $\mu$ m; C, F, I, J: 2  $\mu$ m; D, E: 500 nm; G, H, K: 5  $\mu$ m. Visit [www.nanotomy.org](http://www.nanotomy.org) for browser-based pan-and-zoom analysis of the full resolution datasets

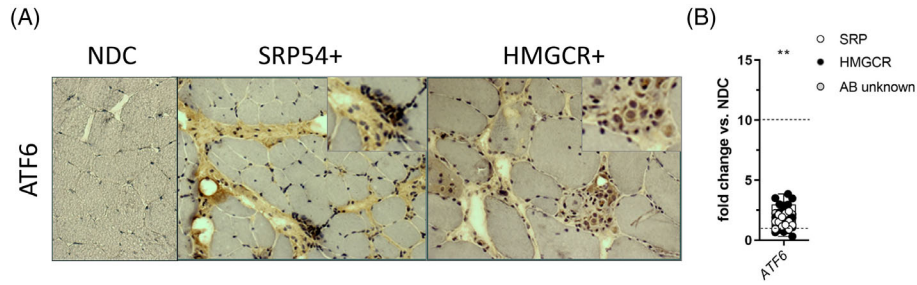


**FIGURE 4** ATF6-mediated unfolded protein response activation is detected in immune-mediated necrotizing myopathies (IMNM) patient's muscles. (A) Immunohistochemical staining reveals accumulation of ATF6 in IMNM patient's muscles predominantly in fibers undergoing myophagocytosis independent of the underlying auto-antibody subtype. Original magnification 400 $\times$ . (B) Gene expression analysis of *ATF6* shows a significant elevation as compared to non-diseased control. The level of significance was set to  $**p < 0.01$

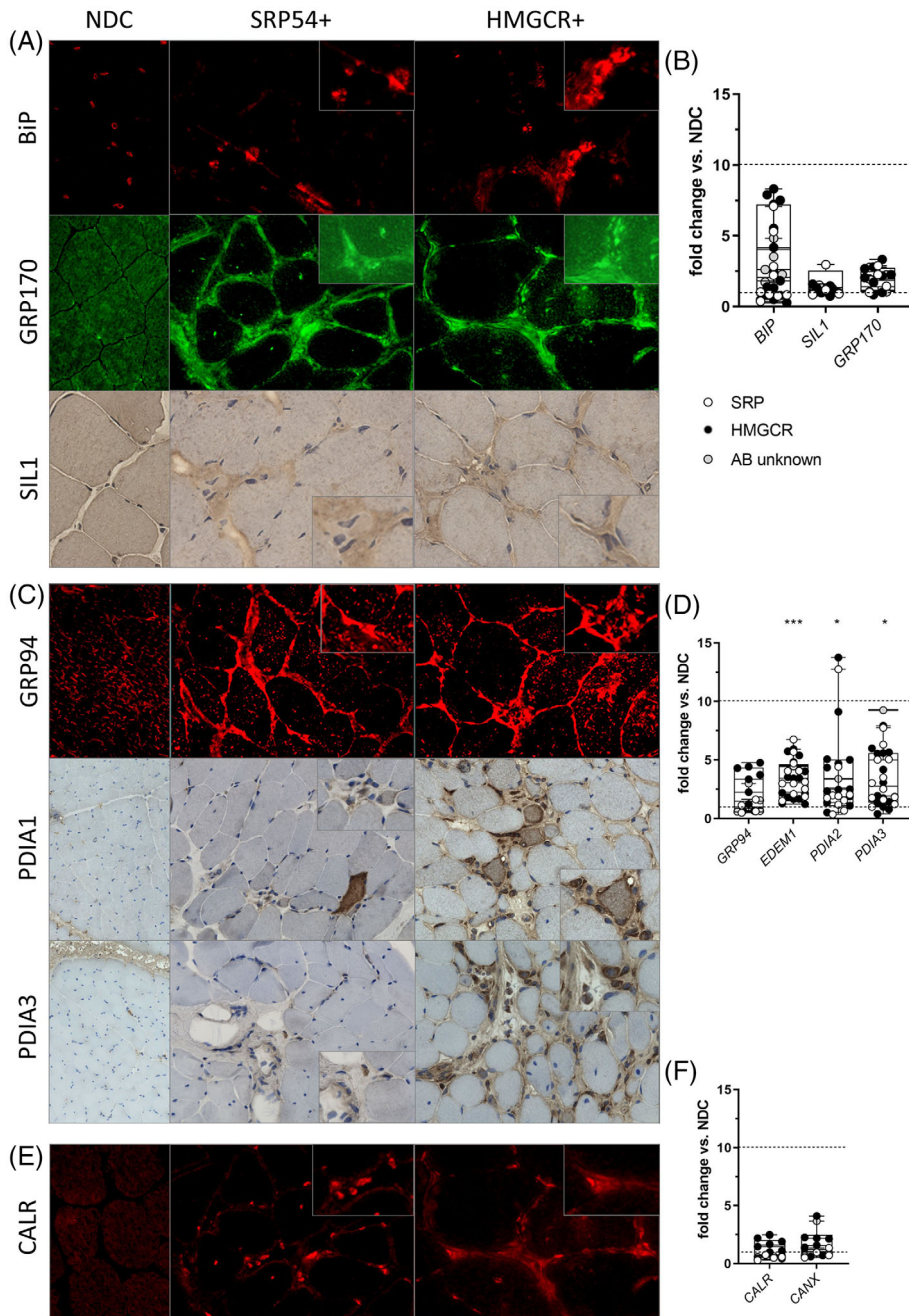


**FIGURE 5** Unfolded protein response-chaperones are activated in immune-mediated necrotizing myopathies (IMNM) patient's muscles. (A) Immunohistochemical staining reveals strong accumulation of BiP and Co-chaperones SIL1 and GRP170/HYOU1 in IMNM patient's muscles independent of the underlying auto-antibody subtype. (B) Gene expression analysis of *BIP*, *SIL1*, and *GRP170* shows no significant elevation as compared to non-diseased control (NDC); however, *BIP* seems to be elevated in single patients. (C) Protein levels of GRP94 were increased on immune cells in the endomysium and on some myofibers, while there was a marked immunohistochemical reaction on myofibers of both PDIs, with subsarcolemmal accentuation for PDIA1. Original magnification 400 $\times$ . (D) Gene expression analysis of *GRP94* showed no significant elevation as compared to NDC, while *EDEM1*, *PDIA2*, and *PDIA3* were significantly elevated in IMNM when compared to NDC. (E) Calreticulin is strongly stained on immune cells. Original magnification 400 $\times$ . (F) Transcriptional analysis showed no elevated expression of *CALR* nor *CANX*. The level of significance was set to  $*p < 0.05$ ,  $**p < 0.01$ ,  $***p < 0.001$

and GRP170 showed the same trend on protein level (Figure 5A), but no profound increase on gene transcript level (Figure 5B), whereby SIL1 increase was detectable in immune but not in muscle cells. Furthermore, MHC cl.-I immune staining was increased sarcolemmally on myofibers adjacent to immune cell infiltrations with intense immunoreactivity of UPR-marker proteins such as GRP170 (see Figure S2).

Next, we analyzed chaperone abundances and distribution focusing on the protein disulfide-isomerase PDI, which is regulated by the three UPR-branches [22]. Fitting to the elevated abundance of pPERK, pIRE1 and ATF6, increased levels of PDIs were identified on both, protein- as well as transcript levels (Figure 5C,D), especially in and around damaged fibers, but did not co-stain with CD68<sup>+</sup>/CD206<sup>+</sup> macrophages (data not shown). The increase of *PDIA2* was significant when compared to expression levels of NDC, while, interestingly, no difference between antibody subgroups was detected.

In addition, we verified the involvement of the lectin-associated chaperones Calreticulin (*CALR*) and Calnexin (*CANX*) on transcript levels: where there was no change detectable (Figure 5F). However, immunofluorescence studies were performed and showed an increase of Calreticulin on protein level in IMNM-patient-derived muscles, whereby no difference between the disease-subgroups was identified (Figure 5E). Furthermore, level of GRP94 (also called Endoplasmic reticulum chaperone), a chaperone functioning in the processing and transport of secreted proteins [22], were studied on transcript and protein level: whereas *GRP94* levels remained largely unchanged, the corresponding protein presents with a subsarcolemmal increase of staining intensity in myofibers of IMNM-patients without differences among the sub-groups (Figure 5C). In line with the presence of ER-stress and UPR-activation, transcript levels of *EDEM1* were significantly increased. The corresponding protein is involved in ER-associated degradation [22].

### 3.4.5 | Comparison to a chronic disease-control group

Besides comparison of IMNM to NDC we included a comparison to a disease-control group consisting of IBM patients, since IBM features a previously studied activation of ER-stress response and UPR activation.

In comparison to IMNM, the IBM group shows a robustly increased gene expression of most of the investigated markers, namely a strong increase of *PERK* and a moderate increase of *EIF2* and *ATF4* (see Figure S3A). Expression levels of *IRE1* and *XBPI* in IBM patients were significantly increased when compared with IMNM and for *XBPI* to NDC (see Figure S3B). Expression of *ATF6* in IBM patients was significantly higher when compared to NDC and IMNM patients (see Figure S3C).

Additionally, most of the chaperones were remarkably increased in the IBM group, reflecting the persisting

involvement of the whole UPR-machinery during IBM disease progression (see Figure S3D).

## 4 | DISCUSSION

Perturbed protein clearance is a pathophysiological hallmark in sporadic inclusion body myositis [24], characterized by accumulation of protein aggregates within muscle fibers and characteristic vacuole formation. In addition, in a previous study we described activation of a highly specific autophagic pathway (CASA) in skeletal muscle tissue of IMNM patients [5]. Moreover, results of our proteomic profiling on IMNM-patients derived skeletal muscles confirmed activation of the protein clearance machinery by increased abundances of proteasomal and autophagic proteins along with cytosolic chaperones. These biochemical findings accord with the results of our ultrastructural studies on IMNM-patients derived muscle biopsies revealing the presence of autophagic vacuoles accompanied by enlarged ER-structures suggesting the presence of ER-stress. Along this line, the same proteomic signature revealed an increase of ER/SR-resident proteins suggesting altered ER/SR-homeostasis. Prompted by these combined morphological and proteomic findings and the facts that ER/SR-stress and UPR activation often precede activation of the autophagic system, we further investigated the presence of ER/SR-stress and UPR-activation in the pathophysiology of IMNM. Results of these combined studies seem indicative of a broad UPR-activation and novel pathognomic feature of IMNM:

### 4.1 | PERK-mediated UPR-branch

PERK (EIF2AK3; eukaryotic translation initiation factor 2-alpha kinase 3) undergoes activation via the luminal domain and activates itself by homo-dimerization followed by autophosphorylation after dissociation of BiP in the presence of ER/SR-stress. This molecular procedure is followed by phosphorylation of eIF2a and activation of ATF4 [22]. Indeed, our combined molecular studies revealed increased phosphorylation of PERK and eIF2a along with increased expression and protein abundance of ATF4 suggestive of the activation of the UPR-branch. It is worth mentioning that increased protein abundance was not identified in muscle fibers but strongly on immune cells (like macrophages) suggesting that this UPR-branch is activated here.

### 4.2 | IRE1-mediated UPR-branch

IRE1 (inositol-requiring kinase 1) undergoes activation via the luminal domain and activates itself by homo-dimerization and autophosphorylation after dissociation

of BiP in the presence of ER/SR-stress. The activated domain splices XBPI (Xbox binding protein) mRNA allowing its ribosomal translation and synthesis of the XBPI transcription factor, XBPI upregulates UPR-modulating factors including chaperones by directly binding to stress element promoters of the corresponding genes within the nucleus [25]. Although our transcript studies did not reveal an increased expression of *IRE1*, increased phosphorylation of IRE1 was identified on immune cells by immunohistochemistry, a finding which is in line with the known activation mechanism of this UPR-modulator [22]. Moreover, *XBPI*-levels are increased, and elevated XBPI protein levels were identified in skeletal muscle of IMNM-patients further suggesting an activation of this UPR-branch, and thus of an UPR-activation on a broader level, an observation, which has already been made in other muscle diseases, featuring an impaired ER/SR-function although based on a genetic defect [7]. Hence, one might speculate that binding of anti-SRP54 and anti-HMGCR antibodies to their target proteins impacts proper functionality of this subcellular compartment, leading to myofiber damage and exposition of the autoantigen—then “visible” for the immune system, which is activated in form of sarcolemmal MHC cl. I upregulation and attraction of phagocytic cells.

#### 4.3 | ATF6-mediated UPR-branch

ATF6 (activating transcription factor 6) is a basic leucine zipper transcription factor [25]. Upon BiP dissociation, ATF6 translocates to the Golgi apparatus. There, the protein undergoes proteolytic cleavage to form a 50 kDa sized active transcription factor that in turn translocates to the nucleus, binding to stress element promoters upstream of genes that are upregulated in the UPR [25]. Our transcript studies revealed an increased *ATF6*-expression, and results of our immunostaining studies confirmed an increased myonuclear immunoreactivity of ATF6 in both SRP54- and HMGCR-positive IMNM-muscles indicating a myonuclear translocation of the cleaved ATF6-form toward the forced transcription of UPR-related chaperones.

#### 4.4 | Downstream factors of the UPR-branches

In accordance with the above-mentioned activation of the three UPR-branches, our molecular data demonstrate a subsequent increase of downstream factors including co-chaperones and chaperones. SIL1 and GRP170 are both BiP co-chaperones controlling its chaperone activity [26]. Although results of our transcript studies did not indicate an increased gene expression of *SIL1*, immunostaining studies show elevated protein in IMNM-patient-

derived muscle biopsies but only on immune cells and not on muscle cells. Thus, the ratio of immune cells versus muscle cells in the total RNA-extracts might explain the fact that *SIL1* was not detected increased on transcript level. Another explanation might be a post-transcriptional activation of this UPR-regulated protein [27] in immune cells implicated in pathogenesis of IMNM. *GRP170* transcript levels were slightly increased only in a proportion of patients (irrespective of the antibody-status), but immunofluorescence studies showed increased protein abundances in muscle cells of all patient-derived biopsies also indicating a post-transcriptional activation of this UPR-regulated protein. Taking a co-chaperone function of GRP170 and SIL1 for BiP into account, this finding indicates that GRP170 might act as the crucial BiP co-chaperone in muscle cells in the context of IMNM. In this context it is important to note that previous studies highlighted beneficial functions of cellular SIL1-increase independent of BiP in the context of neurological diseases [27, 28]. However, the significance of increased SIL1 abundance in immune cells has not been studied on the molecular level yet.

Similarly, GRP94 and Calreticulin, two chaperones known to be controlled by UPR [22] were also increased in muscle fibers of IMNM-patients. Of note, elevated transcript levels were identified for chaperones *EDEM1* and *PDIA2*, which inhibit aggregation of misfolded proteins. Activation of this third UPR-branch confirms the assumption of broad UPR-activation based on anti-SRP54- and anti-HMGCR-antibody binding to the respective SR-resident antigens resulting in perturbed function of this subcellular compartment impacting on general homeostasis as indicated by the results of our proteomic profiling and the findings of our previous study [5] (Figure 5).

In sum, results of our combined transcript and protein studies demonstrate an activation of all three UPR-branches in IMNM which most likely precedes the activation of the protein clearance machinery as hypothesized by us before [5]. Some of the UPR-modulators present without changes on the transcript level but elevated protein levels suggest UPR-modulation also on the post-transcriptional level, for instance by increased half-life-time of these proteins or increased translation of transcripts (visualization see Figure 6). Interestingly, SIL1 presenting with marked staining results on immune cells but not muscle cells may suggest a particular function of this protein in the immune defense mechanism of IMNM rather than in the restoration of muscular protein homeostasis by UPR-activation. Along this line, UPR-activation, for example, GRP94, GRP170, PDIA1, and PDIA3 within muscle fibers might not only serve to restore protein homeostasis, but also to enhance sarcolemmal presentation of proteins, which is crucial for attracting immune cells. We recapitulate previously reported differential involvement of immune cells, mostly macrophages [29], and cells of parenchymal organs [30, 31], by showing

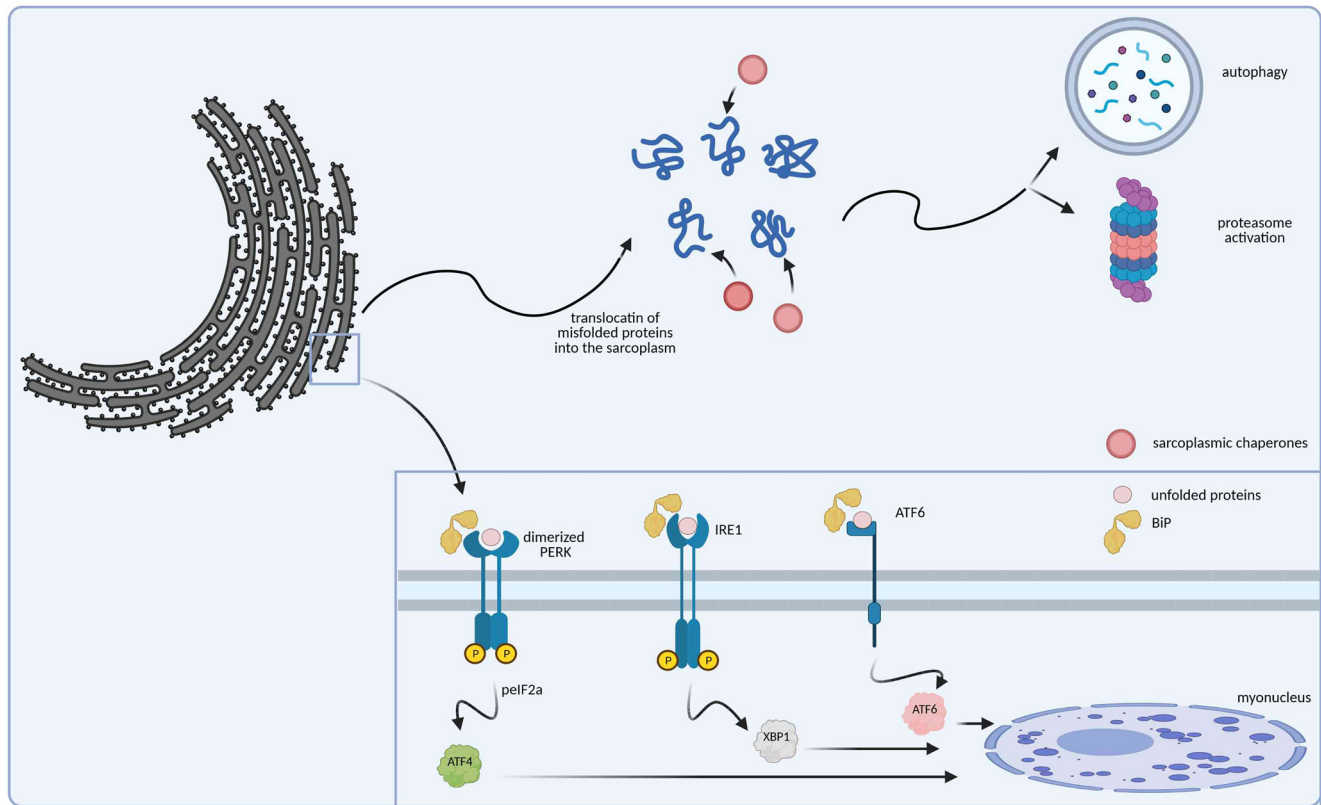


**FIGURE 6** Scheme of perturbed proteostasis leading to activation of the unfolded protein response (UPR) and the protein clearance machinery in muscle cells of immune-mediated necrotizing myopathies (IMNM) patients. Results of combined transcript and protein studies demonstrate an activation of all three UPR-branches in IMNM patient-derived muscle cells, which most likely precedes the activation of the protein clearance machinery. Created with [BioRender.com](https://www.biorender.com)

expression on myofibers of a number of the studied proteins in IMNM. The tight interaction of ER stress in macrophages and cardiomyocytes in experimental myocarditis mirrors our identification of ER stress molecules and chaperones both on immune cells and the myofibers in IMNM as well [32]. ER-stress and UPR activation are pathophysiological features observed in a variety of neuromuscular diseases [33] and our detailed findings add IMNM to the (growing) list of neurological diseases accompanied by ER-stress and altered protein homeostasis. Notably, the extent of activation is moderate and different in comparison to that in myofibers of IBM patients. Hence, we hypothesize that this is at least in part reflected by the fact that IMNM is a subacute disease and muscle biopsy is performed in the very beginning of its manifestation, while there is obvious persistence of its activation over many years in IBM patients' muscles.

Further functional studies (for which suitable in vitro and/ or in vivo models are required) are needed to support the hypothetical model proposed in our study. Nevertheless, given that modulation of ER-stress and UPR via application of chemical chaperones became a promising therapeutic approach in the treatment of different neurological diseases [8], our findings described here might represent the starting point for new interventional concepts.

## AUTHORS CONTRIBUTION

CP, TM, NF Design and conceptualization of the study, acquisition of data, statistical analysis and interpretation of data, drafting of manuscript; AH AS, SL, USS, NM, TR, NFD, JP, AD, NG, HHG, US, YA, OB: revision of manuscript for intellectual content; WS, AR: Design and conceptualization of the study, Interpretation of data, revision of manuscript.

## ACKNOWLEDGMENTS

We gratefully acknowledge the financial support by the Ministerium für Innovation, Wissenschaft und Forschung des Landes Nordrhein-Westfalen and the Bundesministerium für Bildung und Forschung. This work was also supported by a grant of the French Muscular Dystrophy Association (AFM-Téléthon; #23216) to Werner Stenzel and Andreas Roos. Parts of this study were financed in the framework of the NME-GPS project by the European Regional Development Fund (ERDF). Additionally, the authors want to thank the ENMC for organizing IMNM-related workshops. Open Access funding enabled and organized by Projekt DEAL. [Correction added on 21 January 2023, after first online publication: Projekt DEAL funding statement has been added.]

## CONFLICT OF INTEREST

The authors have no conflict of interest.

## ETHICAL STANDARDS AND PATIENT CONSENT

Informed consent was obtained from all patients and the Charité and Essen ethics committees had granted ethical approval.

## DATA AVAILABILITY STATEMENT

The authors of this manuscript state, that they have carefully documented data, methods, and materials used to conduct the research in the article. Data not provided in the article because of space limitations can be made available at the request of other investigators for purposes of replicating procedures and results. Ultrastructural findings by large-scale electron microscopy are openly available on [nanotomy.org](http://nanotomy.org). To our knowledge, there are no legal or ethical reasons or any embargoes on datasets, which may restrict this data availability policy.

## ORCID

Werner Stenzel  <https://orcid.org/0000-0002-1143-2103>

## REFERENCES

- Allenbach Y, Benveniste O, Goebel HH, Stenzel W. Integrated classification of inflammatory myopathies. *Neuropathol Appl Neurobiol.* 2017;43(1):62–81.
- De Bleecker JL, De Paepe B, Aronica E, de Visser M, Group EMMBS, Amato A, et al. 205th ENMC International Workshop: Pathology diagnosis of idiopathic inflammatory myopathies part II 28-30 March 2014, Naarden, The Netherlands. *Neuromuscul Dis.* 2015;25(3):268–72.
- Allenbach Y, Mammen AL, Stenzel W, Benveniste O, Immune-Mediated Necrotizing Myopathies Working G. 224th ENMC International Workshop: Clinico-sero-pathological classification of immune-mediated necrotizing myopathies Zandvoort, The Netherlands, 14-16 October 2016. *Neuromuscul Dis.* 2018;28(1):87–99.
- Knauss S, Preusse C, Allenbach Y, Leonard-Louis S, Touat M, Fischer N, et al. PD1 pathway in immune-mediated myopathies: pathogenesis of dysfunctional T cells revisited. *Neurol Neuroimmunol Neuroinflamm.* 2019;6(3):e558.
- Fischer N, Preusse C, Radke J, Pehl D, Allenbach Y, Schneider U, et al. Sequestosome-1 (p62) expression reveals chaperone-assisted selective autophagy in immune-mediated necrotizing myopathies. *Brain Pathol.* 2019;30(2):261–71.
- Song S, Tan J, Miao Y, Zhang Q. Crosstalk of ER stress-mediated autophagy and ER-phagy: involvement of UPR and the core autophagy machinery. *J Cell Physiol.* 2018;233(5):3867–74.
- Roos A, Buchkremer S, Kollipara L, Labisch T, Gatz C, Zitzelsberger M, et al. Myopathy in Marinesco-Sjogren syndrome links endoplasmic reticulum chaperone dysfunction to nuclear envelope pathology. *Acta Neuropathol.* 2014;127(5):761–77.
- Zito E. Targeting ER stress/ER stress response in myopathies. *Redox Biol.* 2019;26:101232.
- Bravo R, Parra V, Gatica D, Rodriguez AE, Torrealba N, Paredes F, et al. Endoplasmic reticulum and the unfolded protein response: dynamics and metabolic integration. *Int Rev Cell Mol Biol.* 2013;301:215–90.
- Bertolotti A, Zhang Y, Hendershot LM, Harding HP, Ron D. Dynamic interaction of BiP and ER stress transducers in the unfolded-protein response. *Nat Cell Biol.* 2000;2(6):326–32.
- Benbrook DM, Long A. Integration of autophagy, proteasomal degradation, unfolded protein response and apoptosis. *Exp Oncol.* 2012;34(3):286–97.
- Preusse C, Allenbach Y, Hoffmann O, Goebel HH, Pehl D, Radke J, et al. Differential roles of hypoxia and innate immunity in juvenile and adult dermatomyositis. *Acta Neuropathol Commun.* 2016;4(1):45.
- Roos A, Hathazi D, Schara U. Immunofluorescence-based analysis of Caveolin-3 in the diagnostic management of neuromuscular diseases. *Methods Mol Biol.* 2020;2169:197–216.
- Dittmayer C, Goebel HH, Heppner FL, Stenzel W, Bachmann S. Preparation of samples for large-scale automated electron microscopy of tissue and cell ultrastructure. *Microsc Microanal.* 2021;27(4):815–27.
- Cardona A, Saalfeld S, Schindelin J, Arganda-Carreras I, Preibisch S, Longair M, et al. TrakEM2 software for neural circuit reconstruction. *PLoS One.* 2012;7(6):e38011.
- Bankhead P, Loughrey MB, Fernandez JA, Dombrowski Y, McArt DG, Dunne PD, et al. QuPath: open source software for digital pathology image analysis. *Sci Rep.* 2017;7(1):16878.
- Burkhardt JM, Schumbrutzki C, Wortelkamp S, Sickmann A, Zahedi RP. Systematic and quantitative comparison of digest efficiency and specificity reveals the impact of trypsin quality on MS-based proteomics. *J Proteomics.* 2012;75(4):1454–62.
- Vaudel M, Barsnes H, Berven FS, Sickmann A, Martens L. SearchGUI: an open-source graphical user interface for simultaneous OMSA and X!Tandem searches. *Proteomics.* 2011;11(5):996–9.
- Vaudel M, Burkhardt JM, Zahedi RP, Oveland E, Berven FS, Sickmann A, et al. PeptideShaker enables reanalysis of MS-derived proteomics data sets. *Nat Biotechnol.* 2015;33(1):22–4.
- Eskelinen EL. To be or not to be? Examples of incorrect identification of autophagic compartments in conventional transmission electron microscopy of mammalian cells. *Autophagy.* 2008;4(2):257–60.
- Eskelinen EL. Maturation of autophagic vacuoles in mammalian cells. *Autophagy.* 2005;1(1):1–10.
- Walter P, Ron D. The unfolded protein response: from stress pathway to homeostatic regulation. *Science.* 2011;334(6059):1081–6.
- Kopp MC, Larburu N, Durairaj V, Adams CJ, Ali MMU. UPR proteins IRE1 and PERK switch BiP from chaperone to ER stress sensor. *Nat Struct Mol Biol.* 2019;26(11):1053–62.
- Askanas V, Engel WK, Nogalska A. Sporadic inclusion-body myositis: a degenerative muscle disease associated with aging, impaired muscle protein homeostasis and abnormal mitophagy. *Biochim Biophys Acta.* 2015;1852(4):633–43.
- Read A, Schroder M. The unfolded protein response: an overview. *Biology (Basel).* 2021;10(5):384.
- Dudek J, Benedix J, Cappel S, Greiner M, Jalal C, Muller L, et al. Functions and pathologies of BiP and its interaction partners. *Cell Mol Life Sci.* 2009;66(9):1556–69.
- Labisch T, Buchkremer S, Phan V, Kollipara L, Gatz C, Lentz C, et al. Tracking effects of SIL1 increase: taking a closer look beyond the consequences of elevated expression level. *Mol Neurobiol.* 2018;55(3):2524–46.
- Filezac de L'Etang A, Maharjan N, Cordeiro Brana M, Rueggesser C, Rehmann R, Goswami A, et al. Marinesco-Sjogren syndrome protein SIL1 regulates motor neuron subtype-selective ER stress in ALS. *Nat Neurosci.* 2015;18(2):227–38.
- Raines LN, Zhao H, Wang Y, Chen HY, Gallart-Ayala H, Hsueh PC, et al. PERK is a critical metabolic hub for immunosuppressive function in macrophages. *Nat Immunol.* 2022;23(3):431–45.
- Ito H, Yamashita Y, Tanaka T, Takaki M, Le MN, Yoshida LM, et al. Cigarette smoke induces endoplasmic reticulum stress and

- suppresses efferocytosis through the activation of RhoA. *Sci Rep.* 2020;10(1):12620.
31. Bradley KL, Stokes CA, Marciniak SJ, Parker LC, Condliffe AM. Role of unfolded proteins in lung disease. *Thorax.* 2021;76(1):92–9.
  32. Zhang H, Yue Y, Sun T, Wu X, Xiong S. Transmissible endoplasmic reticulum stress from myocytes to macrophages is pivotal for the pathogenesis of CVB3-induced viral myocarditis. *Sci Rep.* 2017;7:42162.
  33. Wehl CC, Udd B, Hanna M, Group Ews. 234th ENMC International Workshop: Chaperone dysfunction in muscle disease Naarden, The Netherlands, 8-10 December 2017. *Neuromuscul Dis.* 2018;28(12):1022–30.

## SUPPORTING INFORMATION

Additional supporting information may be found in the online version of the article at the publisher's website.

**How to cite this article:** Preusse C, Marteau T, Fischer N, Hentschel A, Sickmann A, Lang S, et al. Endoplasmic reticulum-stress and unfolded protein response-activation in immune-mediated necrotizing myopathy. *Brain Pathology.* 2022; 32(6):e13084. <https://doi.org/10.1111/bpa.13084>